Rapid production of β-$FeSi_2$ by spark-plasma sintering

K. NOGI, T. KITA
Joining and Welding, Research Institute, Osaka University, Mihogaoka 11-1, Ibaraki, 567-0047 Japan
E-mail: ktakuji@mac.com

Thermoelectric materials of $Fe_{0.91}Mn_{0.09}Si_2$ were produced with two methods (i.e., hot pressing (HP) and spark-plasma sintering (SPS)) and their thermoelectric properties were compared. The relative density of the samples sintered at the same temperature for thirty minutes was similar. The relative density of the SPS specimen reached 90% in five minutes at 1173 K, while the HP specimen reached 90% in thirty minutes at 1173 K. The optimum condition of the heat treatment was found to be for 3.6 ks at 943 K for the transformation to the β-phase. The peritectoid reaction ($\alpha + \varepsilon \rightarrow \beta$) mainly occurred at and above 953 K, and the eutectoid reaction mainly occurred at 943 K. The β-phase ratio of the HP specimen was larger than that of the SPS specimen because the peritectoid reaction occurred during longer cooling period from 1173 K to 943 K. Consequently, the Seebeck coefficient of the SPS specimen was slightly smaller than that of the HP specimen. However, the figure of merit was very similar because the thermal conductivity of the SPS specimen was smaller than that of the HP specimen. Thus, the SPS method is superior to the HP method with respect to mass-production because the production time is significantly shorter.

1. Introduction

Thermoelectric materials have recently been investigated in various systems. In particular, this iron-disilicide system is an attractive system, because the system can be used in air at high temperatures due to its superior oxidation resistance and the nontoxic and cheap raw materials [1–5]. The phase diagram [6] of the iron-silicon system is shown in Fig. 1. In the iron-disilicide system, the β-$FeSi_2$ phase has thermoelectric properties, although the α-$Fe_{1-x}Si_2$ and ε-FeSi phases are metallic and have very low thermoelectric properties [6, 7]. Kojima *et al*. investigated the optimal annealing conditions [7]. They found two different reaction-mechanisms in the β-phase formation below and above the critical temperature: T_c. One is the ordinary peritectoid reaction of $\alpha + \varepsilon \rightarrow \beta$ above the Tc. The other is a two-stage reaction consisting of the eutectoid reaction $\alpha \rightarrow \beta + Si$ and the subsequent reaction $\varepsilon + Si \rightarrow \beta$ below the T_c. The optimal annealing temperature, T_{opt}, is 1123 K for the pure β-phase and decreases with Mn addition as shown in Table I [7]. β-$FeSi_2$ is generally produced by powder metallurgical method because of its brittleness. Hot-pressing (HP) is a traditional sintering method, and spark-plasma sintering (SPS) has recently been developed as a new method [8–13]. SPS is pressure-assisted sintering with self-heating. A powder is filled into a graphite die and pressed between the upper and lower graphite punches as in the case of hot-pressing, but a pulse voltage is charged with a high current between the upper and lower punches. Fig. 2a and b show schematic diagrams of the hot-pressing and spark-plasma sintering equipment, respectively. Due to self-heating, the spark-plasma sintering method enables powder to be rapidly heated and completely sintered in a very short time [8–13]. It is expected that the spark discharge, which takes place among particles, promotes the diffusion and activates the particle surface. Because the properties of the iron-disilicide system are inferior to one-third of the properties of the Bi-Te system, cheap modules has

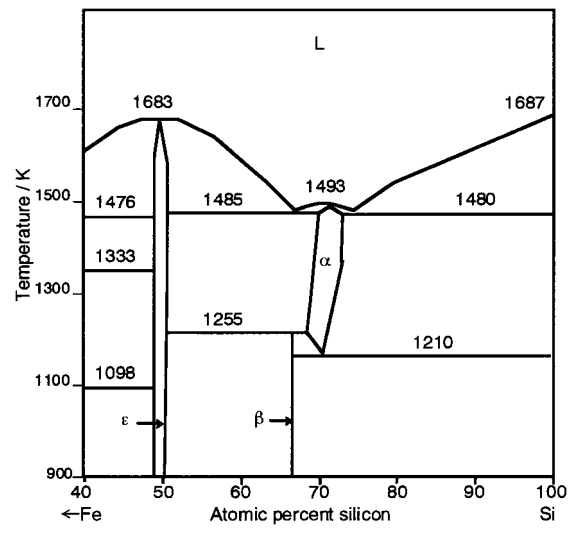

Figure 1 Phase diagram of Fe-Si system.

TABLE I The optimal annealing temperature for $Fe_{1-x}Mn_xSi_2$ after Kojima *et al.* [7]

x	0	0.01	0.02	0.03	0.05
T_{opt}(K)	1123	1122	1113	1110	1095

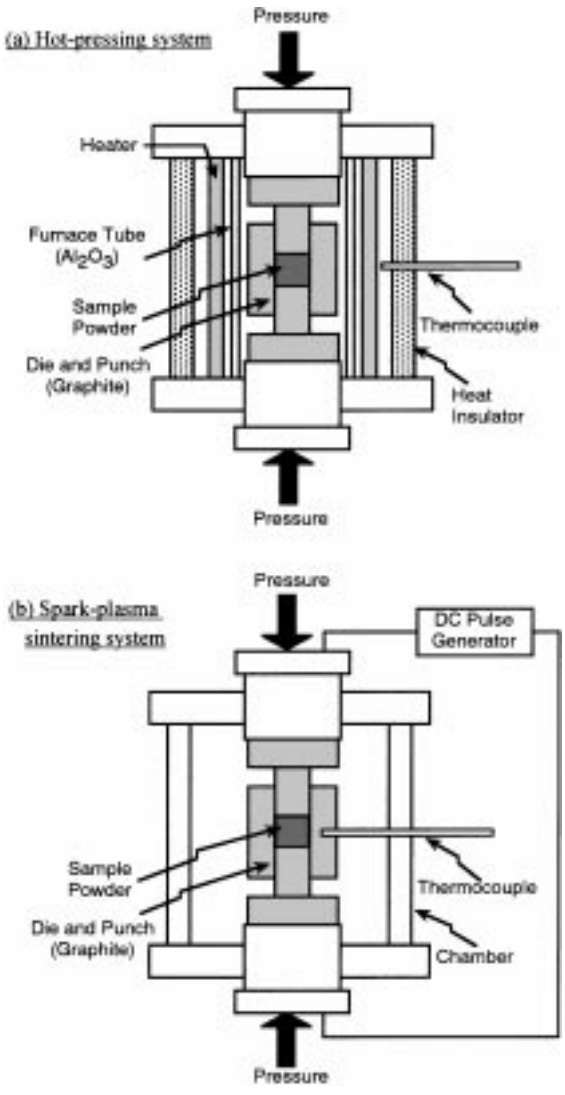

Figure 2 Schematic diagrams of hot-pressing and spark-plasma sintering systems.

to be produced by mass-production. In this study, thermoelectric materials were produced by two methods, HP and SPS, and the possibility of mass-production is discussed.

2. Experimental procedure

The commercially available powder of $Fe_{0.91}Mn_{0.09}Si_2$ (=p-type) (Japan New Metals Co., Ltd.) was used in this study. The mean particle diameter was 1.6 μm. It was filled into a graphite die, and pressed at 25 MPa in a vacuum. The dimension of the hot-pressing specimen is $7 \times 15 \times 4$ mm, and that of the SPS specimen is $\phi 22 \times 4$ mm. In the case of the SPS experiments, a thermocouple for the control of temperature was inserted 5 mm into the graphite die, which had

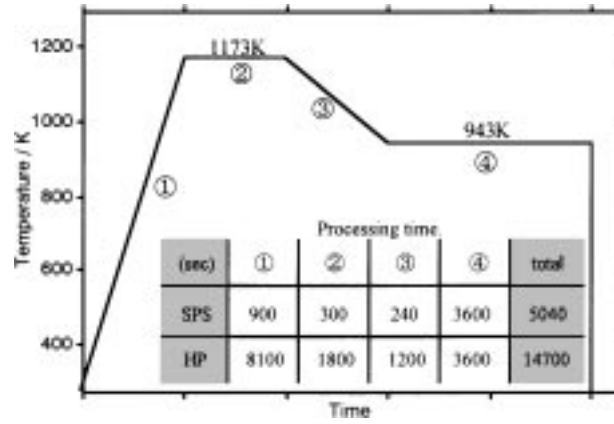

Figure 3 Schematic diagram of the sintring temperature condition.

dimensions of $\phi 44 \times \phi 22 \times 40$ mm. The temperature and the duration shown in Fig. 3 are the optimum conditions as explained later. The phases in the sintered compacts were determined by XRD and the microstructures of the compacts were observed by SEM, and analyzed by EPMA. The Seebeck coefficient and the electrical resistivity were simultaneously measured in the temperature range from 373 K to 1173 K in a vacuum of 10^{-2} Pa. The thermal conductivity was measured with the laser-pulse method in a vacuum of 10^{-2} Pa.

3. Results and discussion

3.1. Densification

First, the relationship between the relative density and the sintering temperature was studied in order to determine the optimum sintering conditions of SPS. The relative density of the samples, which were sintered for 1.8 ks at each sintering temperature without annealing, is shown in Fig. 4. The relative density of the samples sintered at the same temperature for thirty minutes is very similar. Because the specimens often adhered to the graphite punches when the specimens were sintered

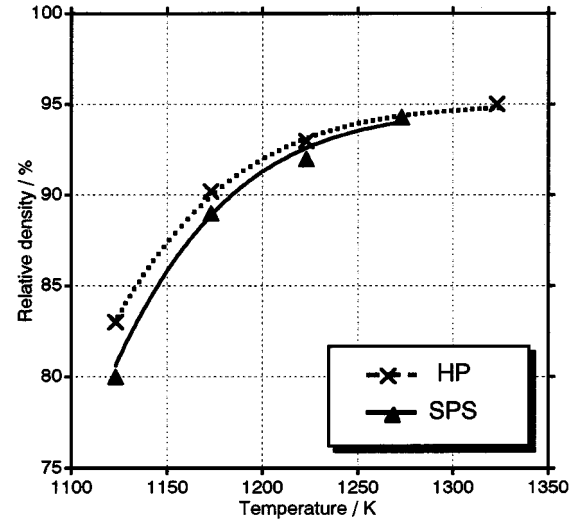

Figure 4 Sintering temperature dependence of relative density of hot-pressing and spark-plasma sintering specimens. Sintering conditions were for 1800 s at 1173 K.

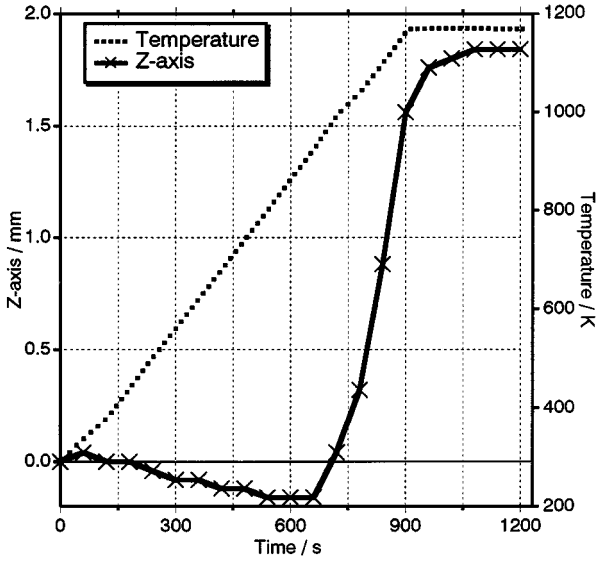

Figure 5 Time dependence of temperature and Z-axis during sintering by SPS.

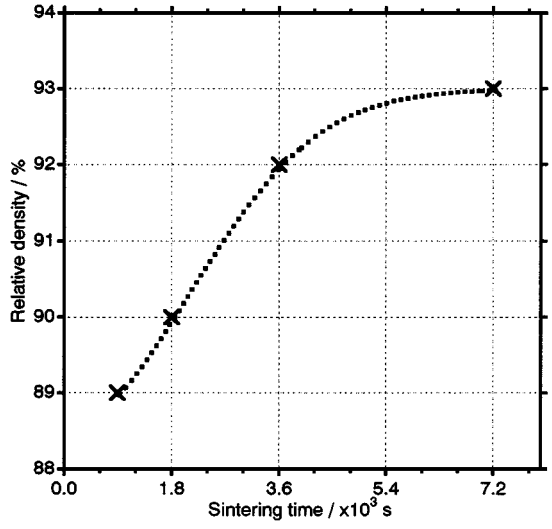

Figure 6 Sintering time dependence of relative density of HP specimen.

by SPS above 1173 K, the sintering temperature of both the SPS and HP was set to be 1173 K. Fig. 5 shows the time dependence of the Z-axis value from the beginning of sintering. The Z-axis value corresponds to the axial displacement of the SPS punch. The Z-axis value increases when the specimen is densified, and it is varied by the thermal expansions of the punches and the specimen. Because the densification finished in 300 s after the temperature reached 1173 K as shown in Fig. 5, and the relative density of the specimen sintered for more than 300 s was the same as that of the specimen for 300 s, the sintering time of SPS was determined to be 300 s at 1173 K. Fig. 6 shows the relationship between the relative density and the sintering time when the HP is performed at 1173 K. The sintering time of the HP was determined to be 1.8 ks because the same relative density as the SPS specimen (=90%) was obtained in 1.8 ks.

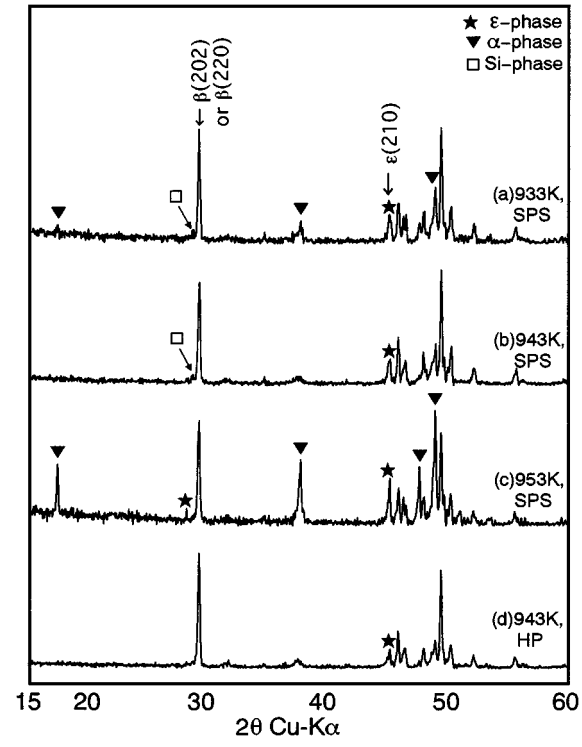

Figure 7 X-ray diffraction patterns of sintered compacts produced under various conditions. (a) SPS specimen annealed at 933 K, (b) SPS specimen annealed at 943 K, (c) SPS specimen annealed at 953 K, (d) HP specimen annealed at 943 K. (The peak without mark is β-phase.)

3.2. Phase and structure

The optimum heat treatment is required for the sintered compacts to be transformed to the β-phase. Fig. 7a–c show the XRD patterns of the SPS specimens that were annealed at 933 K, 943 K and 953 K for 3.6 ks after sintering at 1173 K. In Fig. 7b, strong β-phase peaks and very weak ε-phase and Si-phase peaks were detected. It is clear that the eutectoid reaction of $\alpha \rightarrow \beta + \mathrm{Si}$ and the subsequent reaction $\varepsilon + \mathrm{Si} \rightarrow \beta$ mainly occurred at 943 K. In Fig. 7c, the β-, α- and ε-phase peaks were detected, but the Si-phase peaks were not detected. It can be considered that the peritectoid reaction of $\alpha + \varepsilon \rightarrow \beta$ mainly occurred at 953 K. In Fig. 7a, weak peaks of the α-phase as well as Si-phase peaks were detected. The most likely explanation is that the eutectoid reaction and the subsequent reaction mainly occurred at 933 K, but the decomposition of the α-phase did not finish completely. Fig. 8a and b are reflection electron images of the specimens sintered by SPS. Fig. 8a shows the specimen annealed at 943 K, and Fig. 8b shows the specimen annealed at 953 K. It was revealed by EPMA analysis that the brightest areas were the ε-phases, that of the gray areas were the β-phases, and that the black areas were pores. The composition of the black streaks, which are observed in Fig. 8a and c, was not determined by EPMA because they were too small. However, it should be Si-phases because it was a very Si-rich phase. As shown in Fig. 8a, the ε-phase was covered with the β-phase. The β-phase should be formed by the peritectoid reaction during the cooling from 1173 K to 943 K, and by the reaction of $\varepsilon + \mathrm{Si} \rightarrow \beta$ during the annealing process. It is found that the $\beta + \mathrm{Si}$-phases were outside the β-phase. The $\beta + \mathrm{Si}$-phase should be formed

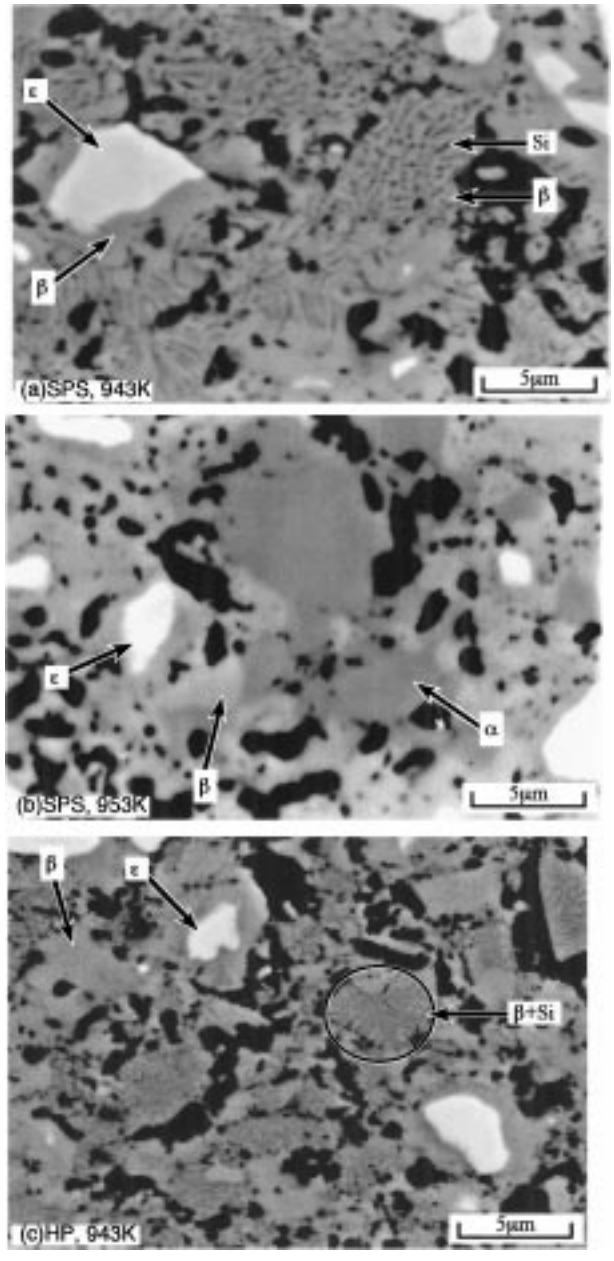

Figure 8 Secondary electron images of (a) SPS specimen annealed at 943 K, (b) SPS specimen annealed at 953 K, (c) HP specimen annealed at 943 K.

by the eutectoid reaction of $\alpha \rightarrow \beta + \mathrm{Si}$. In Fig. 8b, the ε-phases were covered with β-phase layers. Compared with Fig. 8a, the β-phase layers were slightly thicker. However, the α-phases were left outside the β-phase, and no Si-phase could be observed in the α-phases. Judging from these results, it can be concluded that T_{opt} is between 943–953 K for the $Fe_{0.91}Mn_{0.09}Si_2$ material. These values are much lower than those reported by Kojima *et al*. (Table I). It is found from Fig. 7b and c and Fig. 8a and b that the amount of the β-phase formed by the eutectoid reaction was much larger than that of the β-phase formed by the peritectoid reaction at the same annealing time. The annealing conditions of the SPS were determined to be at 943 K for 3.6 ks, as shown in Fig. 3, because the strong α- and ε-phase peaks were detected in the specimen annealed at 943 K for 1.8 ks. The annealing conditions of the HP were set to be the same as the SPS. The specimens, which will be discussed in the following sections, were produced under these conditions.

Fig. 7d shows the XRD pattern of the specimen produced by HP. The peak intensity ratios between $\varepsilon(210)$ and $\beta(220,202)$, that is, I_ε/I_β were measured using Fig. 7b and d. The ratios of the HP and SPS specimens were 0.17 and 0.29, respectively. The reason why a larger amount of ε-phase is left in the SPS specimen than in the HP specimen is because the cooling rate before the annealing was different. In the case of the HP, 1.2 ks was required to cool the specimen from 1173 K to 943 K. However, in the case of the SPS, only 240 s was required for the same amount of cooling. In the cooling period, the peritectoid reaction of $\alpha + \varepsilon \rightarrow \beta$ should have occurred, because the β-phase layer covering the ε-phase was thicker in the HP specimen than in the SPS specimen, which was more rapidly cooled, as shown in Fig. 8a and c. The gray area excluding the black areas in these photographs almost correspond to the β-phase. The ratios of the gray parts in the SPS and the HP sample were 90%, and 95%, respectively. The difference in the grain size was not revealed because the grain boundary was unclear.

3.3. Thermoelectric properties

The temperature dependence of the thermoelectric properties of the SPS and HP samples is shown in Fig. 9. The Seebeck coefficient of the HP sample is slightly larger than that of the SPS sample. The difference in the ε-phase ratio causes the difference in the Seebeck coefficient. It is also found that the electrical resistivity is hardly affected by the difference in the ε-phase ratio. However, the thermal conductivity of the HP sample is larger than that of the SPS sample. It can be assumed that the grain growth in the HP sample progressed further than that in the SPS sample, or the fine silicon dispersions were the scattering centers of the phonons. The figure of merit was calculated from the electrical resistivity, the Seebeck coefficient and the thermal conductivity using the equation of $Z = \alpha^2/\rho\kappa$, and shown in Fig. 9d. The figure of merit of the SPS sample is slightly larger than that of the HP sample.

3.4. Remarkable point of SPS

Tamari *et al*. reported that silicon carbide is densified by SPS at a lower sintering temperature, compared with HP [8]. In this study, the same relative density was also obtained in the SPS, but for a much shorter time. If the sintering time is longer in the HP, the specimens should be more densified. Therefore, it is revealed that the SPS allows the specimen to be sintered at a lower temperature for a shorter time due to the rapid densification, compared with the HP method. Because the thermoelectric properties of the SPS specimens are almost the same as the HP specimens, it is concluded that the SPS method is much superior to the HP method with respect to mass-production.

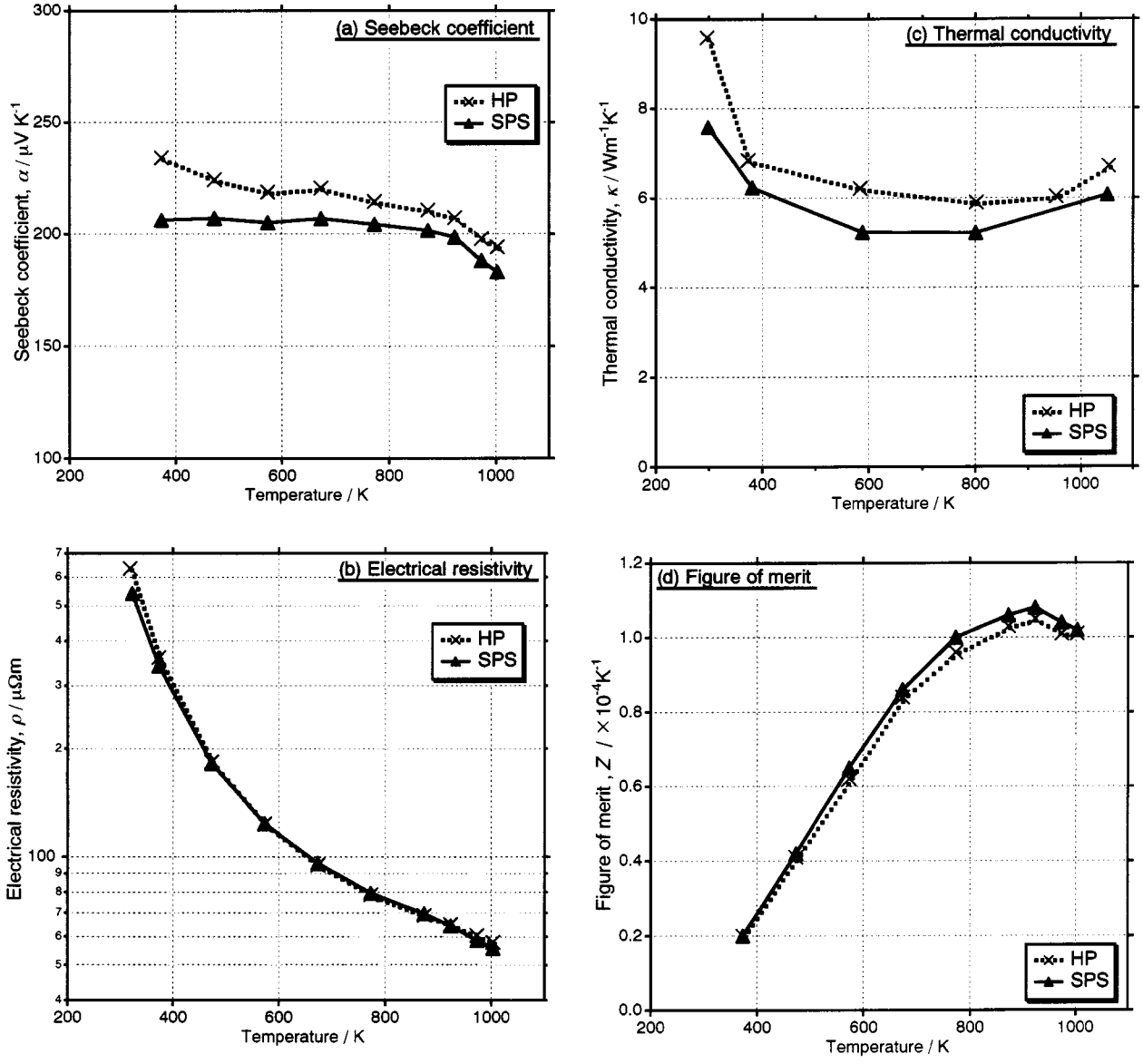

Figure 9 Temperature dependence of thermoelectric properties.

4. Conclusions

(1) Spark-plasma sintering allows thermoelectric materials to be produced very rapidly, and the production time in the SPS method is reduced by one-third when compared for that in the hot-pressing method.

(2) The thermoelectric properties of the specimen produced by spark-plasma sintering are almost the same as those of the hot-pressed specimen.

Acknowledgement

The authors greatly appreciate the supports of Hosokawa Powder Technology Foundation.

References

1. I. NISHIDA, *Phys. Rev. B* **7** (1970) 2710.
2. U. BIRKHOLZ and J. SCHELM, *Phys. Status Solidi* **27** (1968) 413.
3. T. KOJIMA, M. OKAMOTO and I. NISHIDA, in Proc. 5th Int. Conf. Thermoelectric Energy Conv., March 1984, p. 56.
4. H. NAGAI, *Mat. Trans., Jim* **36** (1995) 365.
5. M. KOMABAYASHI, K. HIJIKATA and S. IDO, *Jpn. J. Appl. Phys.* **30** (1991) 331.
6. O. KUBASCHEWSKI, "Iron-Binary Phase Diagram" (Springer-Verlag, New York, 1982) p. 136.
7. T. KOJIMA, M. SAKATA and I. NISHIDA, *J. Less-Common Metals* **162** (1990) 39.
8. N. TAMARI, T. TANAKA, K. TANAKA, I. KONDOH, M. KAWAHARA and M. TOKITA, *J. Cer. Soc. Japan* **103** (1995) 740.
9. T. HO SONG, H. LIM LEE, C. HOON PAI and T. MITSUHASHI, *J. Mat. Sci. Let.* **14** (1995) 1715.
10. K. KUMEDA, Y. NAKAMURA, A. TAKATA and K. ISHIZAKI, *J. Cer. Soc. Japan* **107** (1999) 187.
11. T. TOKIAI, T. UESUGI, Y. ETOH, S. TAMURA, Y. YONEYAMA and K. KOUMOTO, *ibid.* **104** (1996) 837.
12. J. SCHILZ, L. HELMERS, Y. S. KANG, Y. NODA and M. NIINO, in Proc. 16th Int. Conf. Thermoelectrics, Dresden, August 1997, p. 375.
13. T. NOGUCHI, in Proc. 16th Int. Conf. Thermoelectrics, Dresden, August 1997, p. 207.

Received 24 November 1999
and accepted 2 May 2000